14

Biofunctional Xerography

Felix Löffler[1,3], Yun-Chien Cheng[2,3], Tobias Förtsch[3], Edgar Dörsam[2], Ralf Bischoff[3], Frank Breitling[1] and Alexander Nesterov-Müller[1]
[1]Karlsruhe Institute of Technology, Institute of Microstructure Technology,
[2]Institute of Printing Science and Technology, Darmstadt University of Technology,
[3]German Cancer Research Center, Dep. Chip based peptide libraries,
Germany

1. Introduction

Xerography is a well established technology that has revolutionized document processing (Borsenberger & Weiss, 1993). The word "xerography" has its origin from the Greek words "xerox" – dry and "graphos" – writing. In a laser printer, micrometer sized electrically charged toner particles are assembled by means of electric fields on a development drum and afterwards transferred to a substrate. This basic xerographic process, forming arbitrary particle patterns on a substrate, can be exploited to conduct the combinatorial synthesis of peptide arrays. Specially designed bioparticles can be used to transport amino acids to the dedicated synthesis areas and hence, we call our approach "biofunctional xerography".

The increased interest in novel fabrication methods of molecular arrays results from the large application potential in life sciences. The groundbreaking development of high-density oligonucleotide arrays (>40.000 per cm2) boosted the field of genomics both in scientific and in economic terms (Fodor et al., 1991). However, these elegant methods are not suited for the synthesis of peptide arrays, mainly due to increased number of coupling cycles (one cycle per monomer) needed to complete one layer in a peptide array (20 different monomers) when compared to an oligonucleotide array (4 different monomers). Biofunctional xerography resolved this drawback of the lithographical method with only a single coupling cycle per layer (Beyer et al., 2007).

Other methods, based on printing liquids, address the different monomers at once to the support, but all of these methods have to handle tiny droplets in the nano- or picoliter range which tend to evaporate, intermingle with adjacent droplets, or clog the printing mechanics. These difficulties obviously prohibit the use of a piezo- or inkjet printers for the combinatorial synthesis of peptide arrays. Therefore, the available state-of-the-art is still dominated by the 15-years-old SPOT technology that yields until now only 25 peptides per cm^2, at a cost of >5 € per peptide spot (Frank, 1992).

Compared to fluid droplets, solid particles keep their shape, even at the nanometer regime, they do not spread or evaporate during deposition and they do not dissolve previously deposited materials. Furthermore, chemicals and monomers which are embedded inside of the particles are protected against decay (Adler, 1999). This unique property of solid

shared corresponding authors: Alexander.Nesterov-Mueller@KIT.edu; Frank.Breitling@KIT.edu

particles encouraged further research on selective particle deposition with xerographic methods: One of the most impressive among them being nanoxerography (Jacobs & Whitesides, 2001; Jacobs et al., 2002), which demonstrated the possibility of patterning charged submicron particles by the use of conductive stamp generated electric fields in thin PMMA layers. Modifications of this method use an ion beam instead of a stamp to generate latent electric field images (Fudouzi et al., 2002).
The following proposed method of biofunctional xerography for peptide synthesis is based on a computer chip and allows for complete freedom in combinatorial particle deposition, i.e. all arbitrary particle patterns can be deposited on the same substrate. In this chapter we will consider the three basic elements needed for biofunctional xerography: bioparticles, solid phase polymer chemistry with particles and combinatorial particle deposition on a solid support.

2. Bioparticles

2.1 Composition of bioparticles

As mentioned in the introduction, solid particles are used to transfer activated monomers to a synthesis area. In our case, Fmoc protected amino acids are embedded and immobilized in a solid particle matrix. If the particles are deposited and melted at temperatures up to 90 °C, the monomers can diffuse inside the melted matrix and couple to the solid support according to the classical Merrifield peptide chemistry (Figure 1). Thus, the biofunctional xerography exploits the possibility to form peptide bonds in the melted polymer phase at relatively high temperatures.

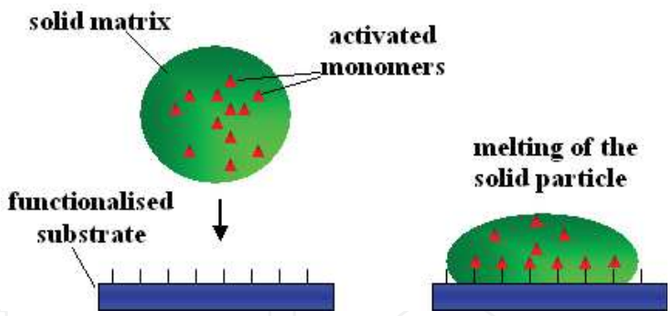

Fig. 1. Solid amino acid particles for combinatorial peptide synthesis

Besides the commercially available standard amino acid monomers suitable for peptide synthesis (Fmoc transient protection group; OPfP ester activation of the C-terminus), the particle composition includes a resin, building the particle polymer matrix and serving for the physical particle stability, charge transfer agents and anti-aggregation components (Table 1). The charge transfer agents provide for the stabilization of the electrical charge on the surface of toner particles.
Indeed, all 20 different Fmoc-amino acids, which have C-terminal OPfp-ester activation groups, proved to be stable for months at room temperature when embedded in the particle matrix, with the single exception of Fmoc-arginine-OPfp. This compound decayed at a moderate rate of 4% per month. It is a remarkable finding, considering that carboxy-activated Fmoc-arginine derivatives are notoriously unstable in other solvents (Cezari & Juliano, 1996).

Component	Function	Relative amount (w/w)
Fmoc-L-aminoacid-OPfpester	Activated amino acid, monomer	10%
SLEC PLT 7547	Resin for physical stability	84.5%
Pyrazolone orange	Charge stabilizer	4.4%
(Fe)2 naphthol complex	Charge stabilizer	1%
Silica particles, Aerosil 812	Anti-aggregation	0.1%

Table 1. Components of amino acid particles (Stadler et al., 2008)

2.2 Generation of bioparticles

In order to produce a toner mass with uniformly dispersed particle components, a mixture of one Fmoc-amino acid OPfp-ester, a polymer and charge stabilizers is dissolved, homogenized and then solidified. The toner mass finally has to be milled with an air jet mill (50AS, Hosokawa). During sieving the milled particles, silica nanoparticles are added which prevents the tendency of particles to agglomerate and enhance their flow ability. The particle size distribution was measured with a Mastersizer (Malvern, type 2000).

Figure 2 shows the air and product transport in an air jet mill 50AS (Hosokawa ALPINE AG & Co. OHG). Small pieces of the mass are introduced into the funnel (a). The drive air (c) is sucked in at the injector (b) and mixed with the raw mass. This mixture is transported to the mill chamber (g). The milling air (d) passes through the air ring (e) and jet apertures (f) to the mill chamber. The particle mass is accelerated by the spiral air jets (h). The milling of the particles occurs by their collision with other particles or with the jet ring wall (i). The fine product leaves the mill trough the outlet (j) in the chamber center. The raw product remains in the chamber and is accelerated again. The separation limit depends on the pressure of the milling air.

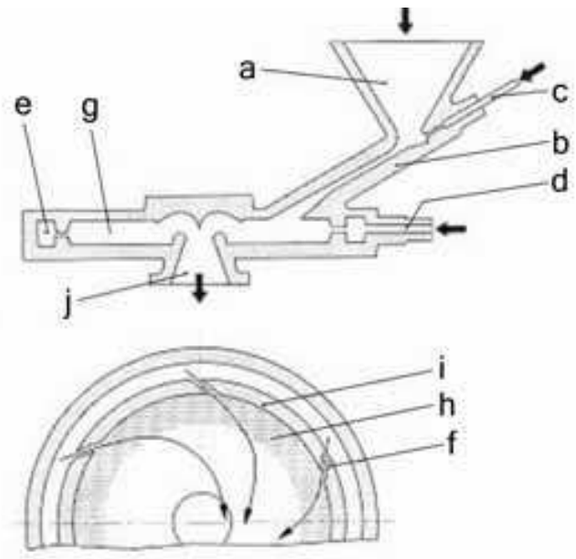

Fig. 2. Air jet mill[2]: funnel (a), injector (b), drive air (c), milling air (d), air ring (e), jet apertures (f), mill chamber (g), spiral air jets (h), jet ring wall (i), outlet (j)

[2] http://www.alpinehosolawa.com

The influence of milling air pressure on particle size is shown in Figure 3. In principle, the higher the milling air pressure is, the smaller is the resulting particle size. This experimental dependence can be derived from the particle separation conditions at the outlet: $F_{cent} = F_d$, where F_{cent} is the centripetal force and F_d the drag force. Since $F_{cent} \sim d^3v^2$ and $F_d \sim dv$, where d is the particle diameter and v the velocity, the relation $v \sim d^{-2}$ results. In this estimate, the relation between the normal and tangential components of the particle velocity in the milling chamber is assumed to be independent of the pressure.

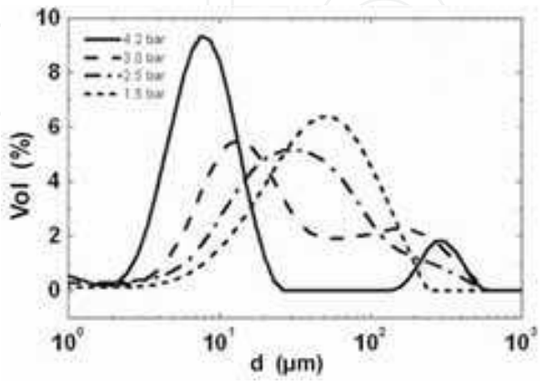

Fig. 3. Distribution of the particle diameter as a function of the milling pressure.

The last expression can be rewritten with the milling pressure as $p \sim d^{-2}$, because v is proportional to p according to the operating manual of the mill. Figure 4 presents the comparison between the obtained dependence and the experimental data, whereby the maximum of the size distribution in Figure 3 is taken as the particle size.

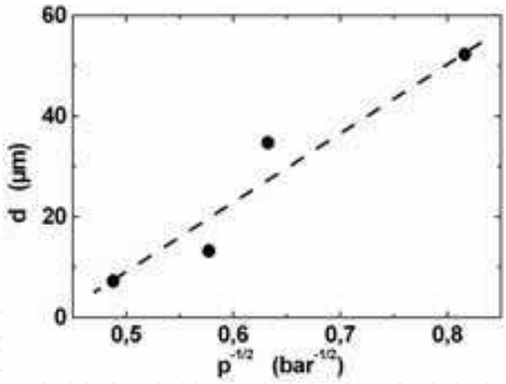

Fig. 4. Maximum values of the size distributions in Figure 3 versus the reciprocal root of the milling pressure ($p^{-1/2}$).

However, this dependence is not valid at higher pressures. Higher pressures do not lead to finer products but rather to a stronger precipitation of the melted mass on the milling chamber wall. Due to the higher kinetic energy of the particles, it is partially converted into heat by inelastic collisions and causes the melting of the particles. Such inelastic collisions occur at critical velocities which are reached by increasing the pressure in the mill chamber. In this case, the size of the milled product depends on the melting point of the different components of the raw mass. The introduction of components with higher melting temperature enables the fabrication of the finer particles in the air jet mill. Further adjustment of the particle size distribution can be realized by sieving.

2.3 Electricity and charge of bioparticles

The q/m-value (the ration of particle charge q and particle mass m) is one of the most important characteristics determining particle behavior in electrical fields. The measurement of triboelectric charging of bioparticles is used for particle characterization and optimization in xerographic processing.

Amino acid type	q/m-value, 10^3 [C/kg]	error stand. deviation	Amino acid type	q/m-value, 10^3 [C/kg]	error stand. deviation
Cys	-3.48	0.70	Val	-1.78	0.26
His	-2.08	0.20	Pro	-1.32	0.11
Trp	-2.05	0.34	Glu	-2.57	0.42
Arg	-1.70	0.31	Ser	-2.28	0.18
Gln	-1.72	0.56	Leu	-2.87	0.24
Phe	-2.55	0.22	Asp	-2.26	0.34
Met	-3.40	0.25	Tyr	-1.79	0.23
Ile	-2.66	0.18	Gly	-1.76	0.33
Thr	-2.14	0.35	Asn	-1.49	0.08
Val	-1.78	0.26	Ala	-1.07	0.27

Table 2. q/m-values of amino acid particles

The set up illustrated in Figure 5 was used to measure the q/m-values of the amino acid particles (Nesterov et al., 2007a, 2007b). This method possesses some advantages over conventional methods based on measuring and collecting the particles in a Faraday cup. The charge of the particles is measured without influencing the particle motion, the measurement is contact-free. Hence, the charging and discharging processes can be monitored during the particle motion. The measurement benefits from the real time data, acquired in the process, because rapid changes in the charging processes occur in less than a second. The particle charge can be measured without any further undesired particle contact with the walls of different tubes before they pass into the filter. On the other hand, a Faraday cup with the particles must be weighed to obtain the particle mass. Since a Faraday cup is made of metal, it is rather heavy. The particle filter in the here presented method can be fabricated of a lighter material, which makes weighing easier.

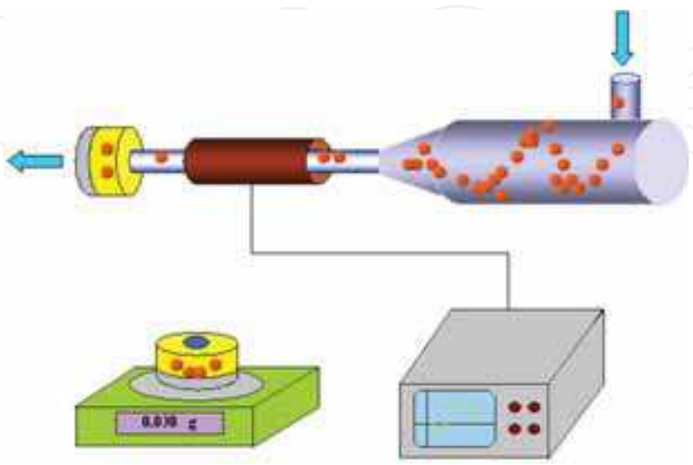

Fig. 5. Measurement of the q/m–values with the inductive cylindrical probe.

The amino acid particles with a relatively narrow size distribution around 10 µm (size distribution generated at a milling air pressure of 4.2 bar, see Figure 3) were electrically activated by contacting the walls of an acrylic glass cone chamber and passed a cylindrical inductive probe into a particle filter. The triboelectric charging of the particles reaches its saturation with an air flow above 30 l/min. The charge of the particle cloud was obtained by the evaluation of the amplitude of the corresponding inductive current. The mass was measured as the difference of the particle filter mass before and after the particles were guided through the experiment. Table 2 summarizes the measured q/m-values for biogenic amino acid particles used in the combinatorial peptide synthesis. The 20 different amino acid particles are composed of similar components: solid matrix, special additives and chemically activated amino acid (see Table 1). The only variable component was the amino acid, which makes up 10% of the composition. This variability and a certain deviation in the mean particle diameter caused the different q/m-values of particles in triboelectric charging. All the amino acid particles have negative q/m-values, which corresponds to the average surface charge densities of $-0.5 \cdot 10^{-5}$ to $-2 \cdot 10^{-5}$ C/m^2. Thus, an activated particle has several thousand elementary charges. It is a rather effective charging process, compared to the critical air breakdown charge density of $\sigma = -2.6 \cdot 10^{-5}$ C/m^2 (Hughes, 1984), at which air breakdown occurs on a conductive surface. Remarkably, the cysteine and methionine amino acid particles, i.e. particles including amino acids with a sulfur atom in the side chain, possess the largest q/m-values.

3. Combinatorial peptide synthesis with particles

The amino acids can polymerize with each other by forming peptide bonds. The peptide bond arises as a result from the chemical reaction between the amino group and the carboxyl group of two different amino acids accompanied by releasing a water molecule (Figure 6). However, it is not trivial to synthesize a defined peptide chain from several amino acids in a test tube. A large number of random oligomers or cyclic bipetides is generated at the simple mixing of activated amino acids.

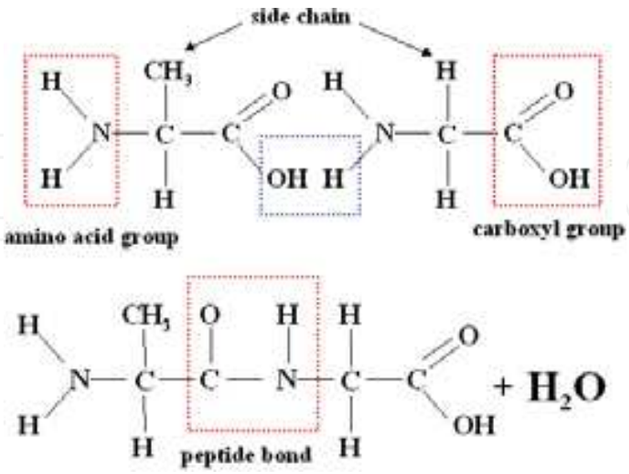

Fig. 6. Formation of peptide bond in reaction between two amino acids

The first synthesis of defined peptides was conducted by T. Curtius at the Ruprecht-Karls-University in Heidelberg in 1881 (Jakubke & Jeschkeit, 1973). The azide-method developed

by him turned out to be of large practical importance. The method utilizes chemical protecting groups for the suppression of uncontrolled formation of peptide bonds. About 50 various protecting group procedures are known today. Nevertheless only a few procedures have been established for routine application.

The invention of the Nobel prize awarded peptide synthesis on a solid substrate (solid phase peptide synthesis) made by R.B. Merrifield at Rockefeller-Institute in New York in 1963 was a breakthrough in peptide chemistry (Merrifield, 1963). The solid phase peptide synthesis enabled routine production of peptides in technical scale for the first time.

Figure 7 schematically shows the principle of the Merrifield synthesis (Koch & Mahler, 2002). The method consists of binding an amino acid by its C-terminal carboxyl group to the insoluble polymer and consequent assembling of the peptide chain at the N-terminal end. Each cycle begins with the removal of the protecting group and results in the growth of the peptide chain by one further amino acid. The multiple repetition of the cycle leads to the synthesis of amino acid chains. Some amino acids possess side chains with hydroxyl, amino or carboxyl groups, which must be chemically neutralized by special protecting groups during synthesis. After the complete synthesis of the peptide, these protecting groups are removed with one chemical step.

Two main peptide synthesis strategies are distinguished according to the kind of protecting groups: Fmoc-(9-fluorenylmethyloxycarbonyl) and BOC-(tert-butyloxycarbonyl) synthesis. The BOC protecting group can be removed with TFA (trifluoroacetic acid) solution without influence on side chain protecting groups of the benzyl type. Finally, the side chain protecting groups are detached with HF (hydrofluoric acid). The BOC strategy goes back to Merrifield. Fmoc synthesis is a chemically milder procedure. The Fmoc protecting group can be removed with a mild base, as a rule piperidin, and is stable in strong acids like TFA or HBr.

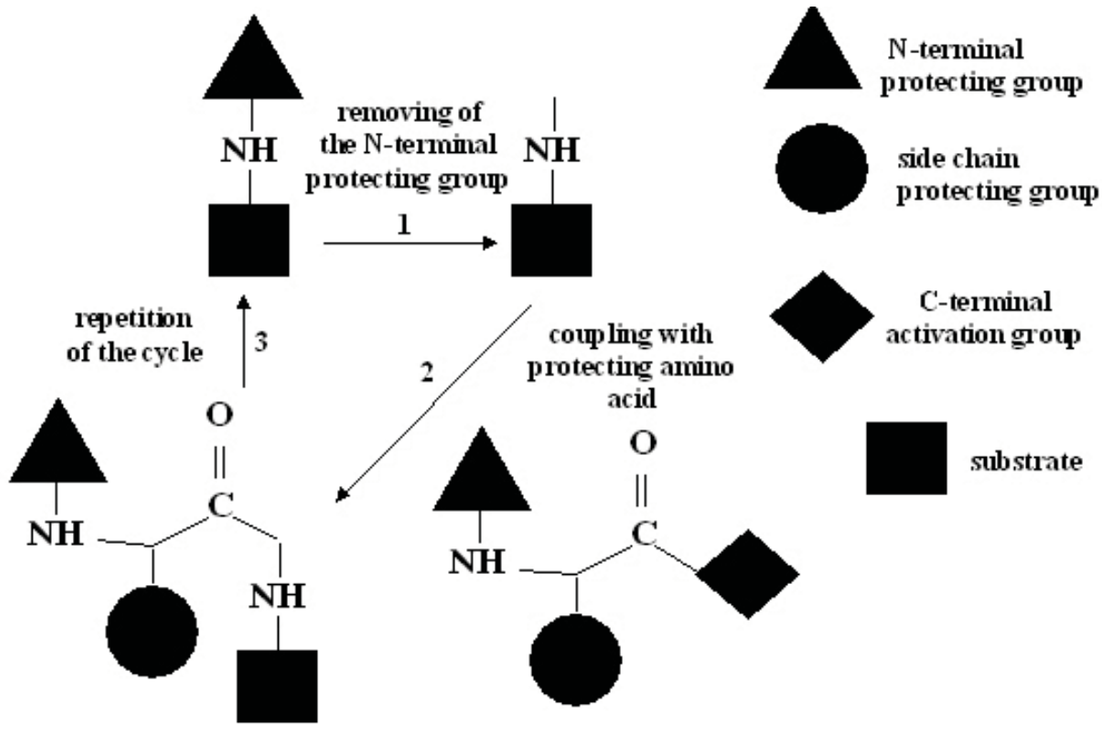

Fig. 7. Solid phase peptide synthesis cycle

The main advantage of the solid phase peptide synthesis is that one can omit the complex cleaning procedures. The removal of reagent excesses and byproducts is carried out through the washing of the substrate, whereas the main product remains on the substrate. Repeatable work cycles allow for automation.
The possible aggregation of growing peptide chains is one of the limits of the solid phase synthesis. Due to the formation of peptide chain loops, ends become inaccessible and further assembly of the peptide strand is impossible. The reason for these side reactions are hydrogen bonds and hydrophobic interactions. Some amino acids like alanine, valine, isoleucine, asparagine and glutamine favour such side reactions. Thus, the synthesis of peptides with more then 15-20 amino acids becomes difficult.
Particle based peptide synthesis has, albeit pursuing the same chemical reactions, several special features: the chemical reaction occurs in the melted polymer matrix with a limited diffusion and this polymer matrix has to be removed during the washing step after coupling amino acids to the surface.
Figure 8 illustrates the principle of the particle based peptide synthesis. First, toner particles with a diameter of about 10 µm, imbedding different activated amino acids into the polymer matrix, are deposited onto a substrate with free amino groups on the surface (Figure 8a). The transition of the particles to a gel-like phase allows for the diffusion and coupling of the imbedded amino acids to the surface (Figure 8b). Thereby, the standard Merrifield peptide synthesis is initiated by melting the particles. This results in an excess of soluble monomer over free amino groups on the array support (~15 nmol free amino groups per cm^2). The coupling step is conducted for 90 min at 90 °C. Afterwards, particle matrix and uncoupled amino acids have to be washed away with DMF (dimethylformamide) (Figure 8c). The next step provides for the removal of the N-terminal protecting groups of the amino acids with 20% piperidine diluted in DMF (Figure 8d). Finally, the support is cleaned with DMF and methanol, before the next layer of amino-acid-particles is deposited on the dried array. Eventually, these steps are repeated layer by layer until the final peptide array is rendered (Figure 8e, f). The side chain protecting groups are removed by washing the array for 2 hours in 91% TFA, 4% DCM, 3% triisobutylsilane, and 2% H_2O (Jones, 2002). The completed peptide array is rinsed with methanol and dried in a stream of nitrogen.

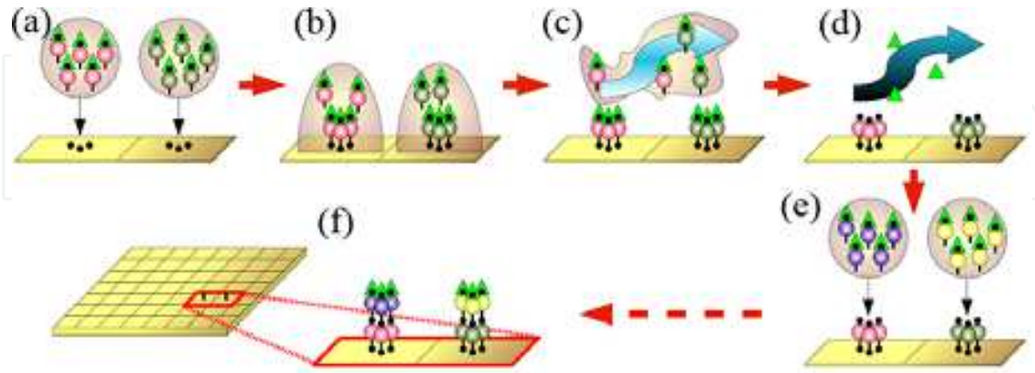

Fig. 8. Schematic peptide synthesis: First, the particles are transferred to a substrate (a). Each particle type imbeds a different amino acid. Afterwards, the particles are melted and the amino acids couple to the surface (b). Then, excess particles and amino acids are washed away (c) and finally, the protective groups are removed (d). The process can be repeated with different particle patterns, until the desired peptide array is completed (e, f).

As the particles can be deposited on glass supports or silicon wafers, a wide choice of chemical methods is available to produce polymeric films with N-termini as the starting points for peptide synthesis. Depending on the desired application, those can be monolayer or polymeric films.
In principle, the biofunctional xerography can be adopted for the synthesis of any artificial polymer such as peptoids, oligocarbamates or oligourea, where the protection group strategy is applicable.

4. Combinatorial particle deposition on microelctronic chips

4.1 Particularities of selective deposition of particles on chips

The key element of biofunctional xerography is the combinatorial particle deposition that allows for significant reduction of the number of chemical cycles. The complexity of the produced peptide array is determined by the complexity of the deposited particle patterns. Combinatorial deposition means that many kinds of particles can be deposited on the same substrate. Our approach uses microelectronic chips on which surfaces electric field patterns can be generated. In this section, we will consider results of experiments and simulations on precise particle deposition on these chips, proof-of principle peptide synthesis and a xerographic technique based on a CMOS chip as a printing head.
An electronic microchip can be used for generating a particle pattern. Figure 9 illustrates the application principle of the chip for combinatorial solid phase peptide synthesis. Several kinds of amino acid particles are selectively deposited according to the consecutively generated electric field patterns (a)-(d). After the completed deposition of a particle layer, the layer is melted (e). The coupling of amino acids occurs during the melting procedure. The matrix substance and the rest of the uncoupled amino acids are removed by washing (e). The chip is then ready for the combinatorial synthesis of the next amino acid residue layer (f). High electric fields emanating from the chip are required to overcome the forces participating in the transport. Such chips can be fabricated routinely in the framework of the commercially available high voltage chip technology according to the design rules. Modern high voltage technologies enable the integration of high and low voltage transistors, such that the sequence of generated patterns can be completely automated.

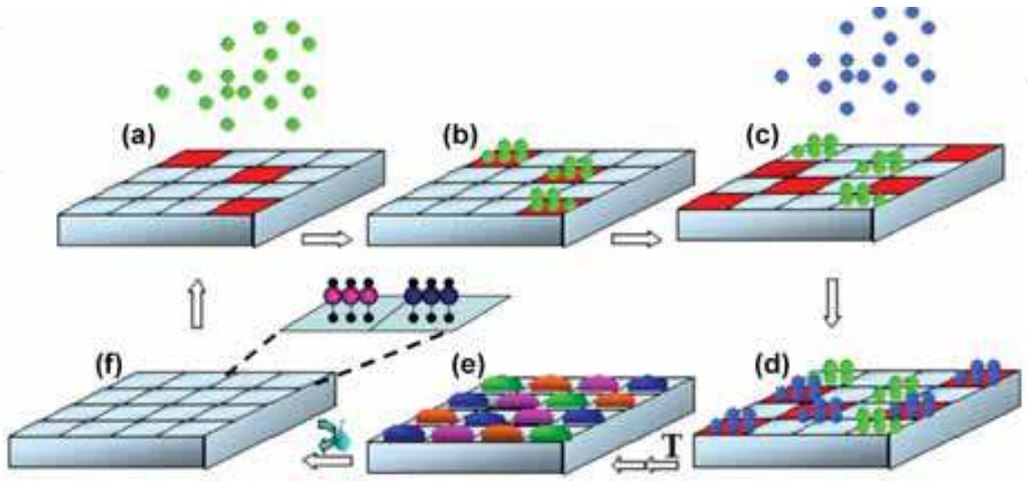

Fig. 9. Solid phase peptide synthesis on the electronic microchip

In comparison to nano particles, micro particles are rather heavy, no Brownian motion occurs in air. Their motion is mainly determined by the drag force and, in absence of the drag force, also by the gravitational force. Therefore the amino acid particles can be transported with the air stream to the chip surface. The transport forces must be smaller than the selective electrical forces on the chip surface. It is known that adhesion forces are relatively large especially for particles with a diameter below 10 µm (Novick et al., 1989; Desai et al., 1999). The addressing of amino acid particles onto the chip is conducted onto a chemically modified surface. The chip surface is coated with a polymer layer, which is necessary to start the peptide synthesis (see section 3). Thus, one must take into account the influence of those layers on the adhesion and electrical forces.

4.2 Microelectronic chips

Two passive chips (without transistors) with a pixel to pixel raster of 100 and 50 µm were fabricated at the Institute for Microelectronics Stuttgart (Figure 10). The chips have the following structure: (1) Si-Wafer; (2) metal layer I (AlSiCu 800 nm); (3) insulator (1000 nm SiO2); (4) metal layer II (AlSiCu 1000 nm); (5) Passivation (550 nm SiO2+ 300 nm Si3N4). A grid electrode on the chip (between two pixels) serves for electrical shielding purposes. The passive chip has pixels with a window above the pixel electrode. Thus, the peptide synthesis is conducted on an aluminum surface. The passive chips allowed only for a limited number of electric field patterns. A chess board like pattern was originally used to study the particle transport processes and for a proof of principle peptide synthesis with solid particles (Nesterov et al., 2010).

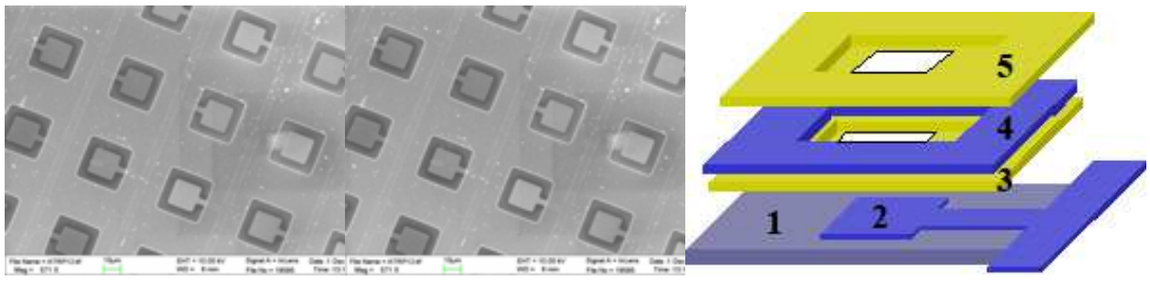

Fig. 10. Fragment of a passive chip (left). Pixel of the passive chip (middle) and its schematic structure (right)

The full combinatorial freedom can be achieved if the voltage can be applied on each pixel separately. A microelectronic chip with such function was designed in a high voltage CMOS (Complementary Metal Oxide Semiconductor) process (König et al., 2010). The total silicon area of the chip is 19.9mm×19.0mm. It is mounted on a PCB support with the dimensions of a standard microscope glass slide (75.8mm×25.9mm×1.0 mm) (Figure 11). The array of 128×128 pixel electrodes (16,384 potential synthesis spots) is located in the center of the chip. Voltages of up to 100 V can be applied independently on each pixel electrode, i.e. arbitrary combinatorial electric field patterns can be generated on the chip surface.

Figure 12 schematically shows the circuit of the HV part in the fabricated CMOS chip. This circuit is a voltage divider, which determines the voltage at the pixel electrode through the gate-source voltage V_{GS} (0 or 5 V). In the case of 0 V, the resistance of the HV-NMOS transistor R_{TR} is significantly larger than the constant resistance R in the circuit and therefore the voltage of 100 V is applied to the pixel electrode. In the case V_{GS} = 5 V, R_{TR} << R and the

pixel electrode is grounded. The resistance R is obtained by using a PMOS-transistor in the chip. The gate voltage of the PMOS transistor was fixed to a bias voltage close to its threshold voltage. The HV part was connected to the LV part through the gate of the HV-NMOS transistor which enabled the programmable control of the voltage VGS and consequently the voltage at the pixel electrode.

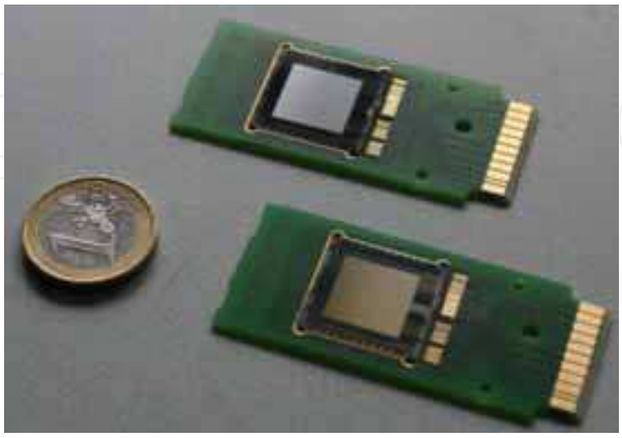

Fig. 11. CMOS chip for peptide synthesis

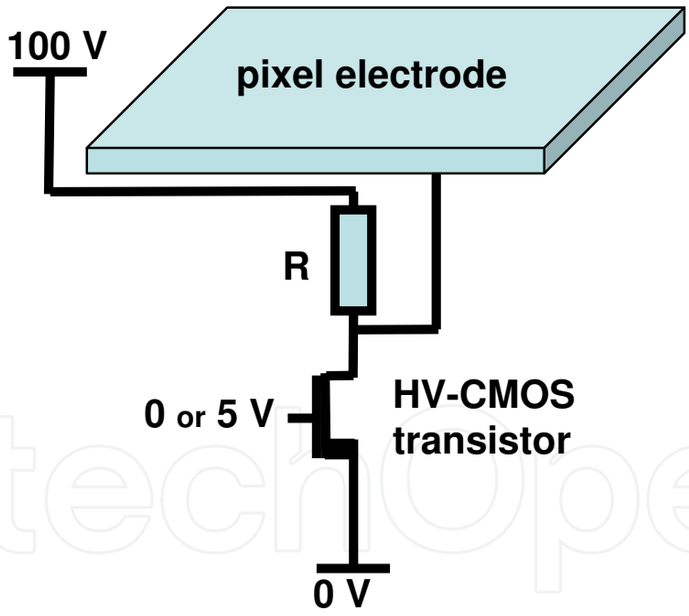

Fig. 12. Principle of the circuit used in the HV part of the CMOS chip

4.3 Particle deposition on microelectronic chips

4.3.1 Forces participating in particle deposition

The forces participating in the particle transport and their deposition are shown graphically in Figure 13. The image force $F_{img} = q^2 / (4\pi \varepsilon_0 d^2)$, which results from the interaction of the particle charge with the metal chip surface, and the gravitational force $F_{grav} = m \cdot g$ can be neglected, being at least one order of magnitude smaller than the drag force and the

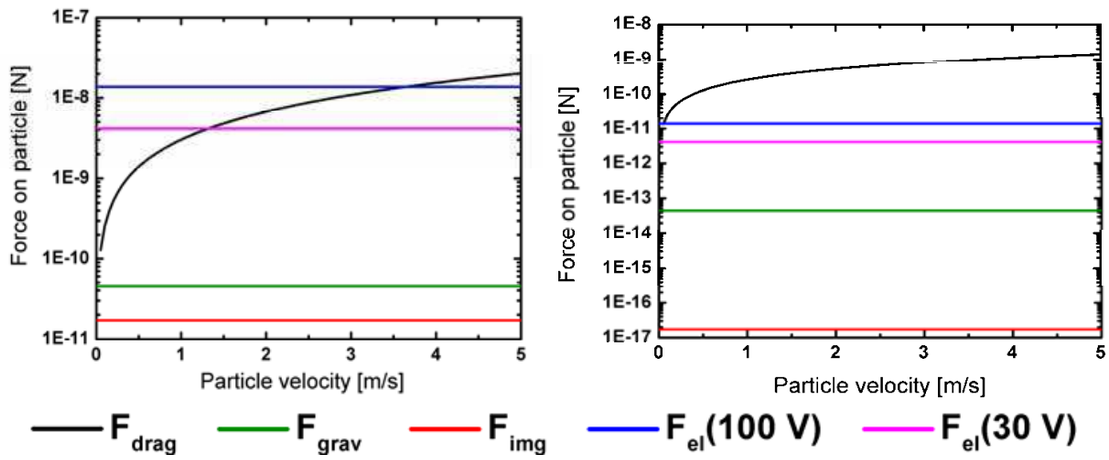

Fig. 13. (left) Forces in the deposition process acting on an aerosol particle with the diameter of 20 µm in a distance of 100 µm from the chip surface; (right) forces as in the latter but for a particle diameter of 2 µm.

electrical force. A particle mass density of 1100 kg/m³ was used to estimate the gravitational force. A q/m-value of $3 \cdot 10^{-3}$ C/kg was chosen for the estimation of the electrical force $F_{el} = E \cdot q$ (with E = U/L) resulting from a pixel electrode with the length L and the voltage U. We estimated the electric force for two different pixel voltages: 30 V and 100 V.

The drag force basically depends on the particle size and on the respective velocity between a particle and the surrounding air. For further calculations and simulations, we use the Khan-Richardson (Coulson & Richardson, 1999) force F_{KR} instead of the standard drag force F_{drag}, which is a good approximation of the drag force for a wide range of particle diameters.

$$F_{KR} = \pi / 4 \cdot d^2 \rho_{air} \cdot \left| v_{air} - v_{part} \right| \cdot \left(v_{air} - v_{part} \right) \left(1.84 \left(Re_{part} \right)^{-0.31} + 0.293 \left(Re_{part} \right)^{0.06} \right)^{3.45}, \quad (1)$$

$$\text{with} \quad Re_{part} = \left| v_{air} - v_{part} \right| \cdot d \cdot \rho_{air} / \eta_{air} \ . \quad (2)$$

d is the particle diameter, v_{part} and v_{air} are the corresponding velocities of the particle and the surrounding air that can assumed as a laminar fluid with the dynamic viscosity η_{air} and the density ρ_{air}.

If we assume that particle movement does not influence the surrounding air flow and if particle-particle interaction (e.g. collision) is negligible due to a low aerosol density, we can limit the calculations of the forces acting in particle deposition to two forces: the Khan-Richardson force and the electrical force.

4.3.2 Simulation

Using this approach, simulations of the particle deposition process can be used to improve the deposition quality and significantly reduce contaminations (Löffler et al., 2011). Especially the particle parameters like charge and size are the key players in spatial defined particle deposition.

The following simulations for particle deposition analysis were obtained with the commercially available program COMSOL Multiphysics (COMSOL, Inc., USA), a finite

element analysis solver, and simulation software. First, the stationary Navier-Stokes equation for the incompressible airflow and the Poisson equation for the electrical field on the chip surface were solved. Then, the particle trajectories were simulated, established on the solutions for the air velocity field and the electrical field.
A two-dimensional simulation model has been designed to investigate the particle dynamics. As shown in Figure 14, particles with a predefined size and negative charge can be attracted by the electrical field of the chip. The chip is modeled by two active pixels set at 100 V separated by three inactive pixels at 0 V each. The electrical fields between chip and sieve selectively guide the aerosol particles to the activated deposition areas. We experimentally verified that the more pixels are switched off in a voltage pattern on the chip surface, the more contaminations on these pixels can be observed after deposition.

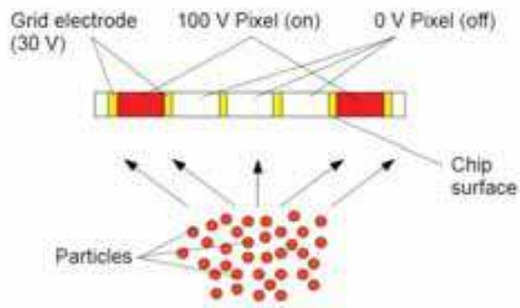

Fig. 14. Schematic particle deposition on a chip; particles move towards the chip and are manipulated by electrical fields resulting from the voltage pattern on the chip surface to enable spatial defined particle deposition

To investigate the causes of contamination, a pattern was modeled which consisted of two active pixels separated by seven inactive pixels as this combination showed a high probability of contamination.
Particles were injected into the air stream in a distance of 1 cm away from the chip surface with an initial particle and air stream velocity of v_0 = 1 m/s in chip direction. The exponential decay of the electrical field intensity emanating from the chip confines the region of interest, where the selective effect of the chip is dominating particle manipulation. Therefore, this region extends only 200µm from the chip surface, as the subsequent simulations demonstrate.
We systematically varied the charge per mass ratio (q/m value) of the particles and the particle diameter in the simulations. Pixel voltages on the chip were set to either 100 V, which yields the highest possible electrical attraction, or to 0 V, to obtain minimal attraction. The voltage of the grid electrode was set to 0 V (Figure 15a) or 30 V (Figure 15b).
The grid electrode plays an important role in particle deposition: In Figure 15, particle trajectories are represented as black lines and the electrical potential in V is shown in grey scale. Above the trajectories, the voltage pattern of the chip surface is indicated (similar to Figure 14). Two pixels are switched to 100 V and in between, seven grounded pixels are located.
Figure 15 shows the simulation of particles with a diameter of 10 µm and a q/m value of $-3 \cdot 10^{-3}$ C/kg. In Figure 15a, the grid electrode is grounded and the particles reach the chip surface. Several of them are not only deposited on the grid electrode, but also on the grounded pixels, causing contaminations. In contrast to this, Figure 15b shows the same

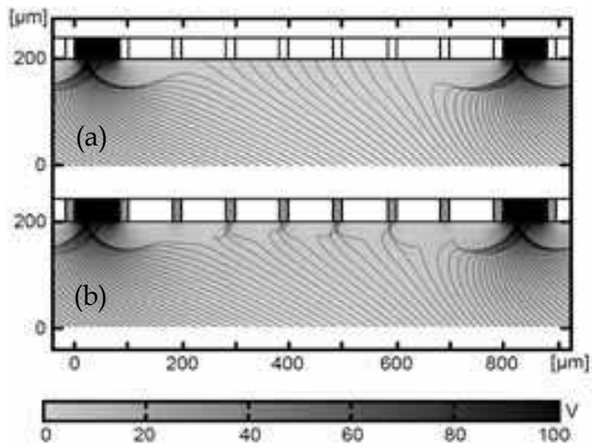

Fig. 15. Simulation of particle deposition on a chip; particles are 10 µm in diameter and feature a q/m value of $-3 \cdot 10^{-3}$ C/kg; (a) the voltage of the grid electrode is 0 V, several particles are deposited as contaminations on deactivated pixels; (b) voltage of the grid electrode is 30 V, excess particles are solely deposited on the grid electrode (Löffler et al., 2011) (Reprinted with permission)

configuration, but the grid electrode is set to 30 V. Here, particles, which are not deposited on the desired pixels, are solely deposited on the grid electrode. Therefore, the grid electrode serves as an adsorber for excess particles, as long as not too many particles accumulate on the grid electrode. This effect is important for contamination free particle deposition. Thus, in all further simulations, the grid electrode is set to 30 V.

4.3.3 Effect of the particle diameter on deposition

The particle size has an abundant effect on the selective particle deposition. In Figure 16, the particle size was altered between 3 and 10 µm ((a) 3 µm; (b) 5 µm; (c) 10 µm) and the charge per mass ratio (q/m value) of the particles was defined as $-3 \cdot 10^{-3}$ C/kg in all three cases.

As shown in Figure 16a, the simulated deposition features very few overall deposition events on the chip surface. In Figure 16b and c, the total number of deposition events rises with particle diameter (i.e. increased number of trajectories). All particles are deposited either on the 100 V pixels or on the grid electrode, which resembles the ideal and desired deposition pattern.

In contrast to these simulations, experiments exhibit a crucial difference: Particles with a mean diameter of 10 µm or greater tend to cause contaminations; they are deposited on both active and grounded pixels.

Hence, the q/m value was altered in one order of magnitude. In Figure 17, all initial conditions were kept as in Figure 16, but a q/m value of $-3 \cdot 10^{-2}$ C/kg was used. The overall number of deposition events on the chip surface has risen because the particles experience a higher attract ion due to the higher q/m value. In Figure 17a and b the particle deposition is still as desired, without contamination. In the case shown in Figure 17c, many particle trajectories end on grounded pixels, indicating contamination. However, due to the lack of adhesion forces, some trajectories near the 100 V pixels are making unrealistic bends near the chip surface. Nevertheless, significant conclusions can be derived from these simulations.

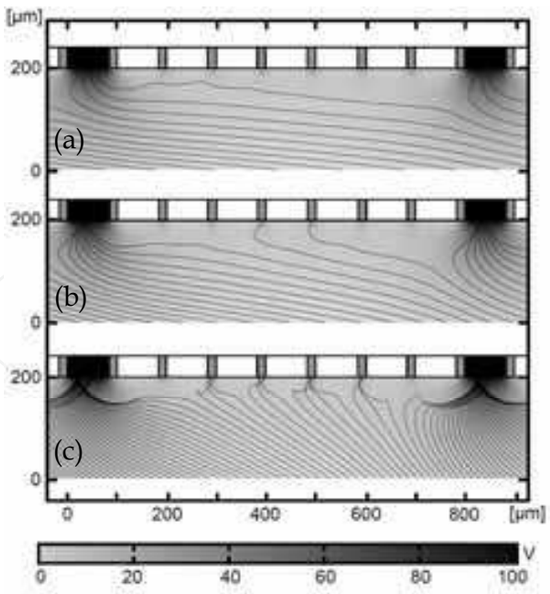

Fig. 16. Simulation of particle deposition on a chip; particle trajectories are represented as black lines, grayscale represents the electrical potential [V]; particle diameters are (a) 3 µm, (b) 5 µm, (c) 10 µm; with q/m value of $-3 \cdot 10^{-3}$ C/kg; in all cases no contamination on grounded pixels occurs (Löffler et al., 2011) (Reprinted with permission)

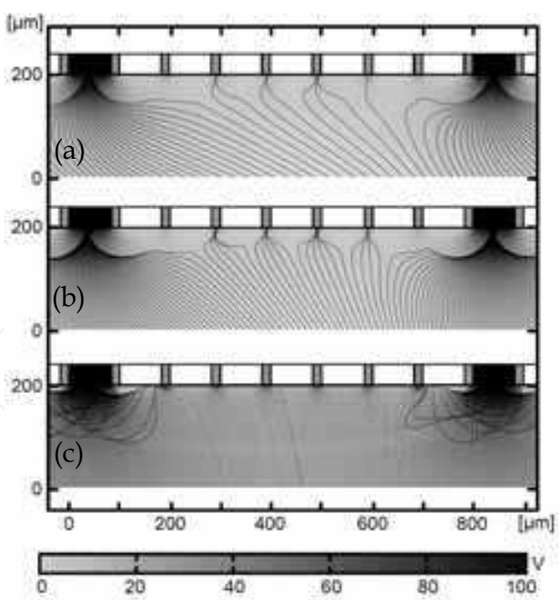

Fig. 17. Simulation of particle deposition on a chip; particle trajectories are represented as black lines, grayscale represents the electrical potential [V]; particle diameters are (a) 3 µm, (b) 5 µm, (c) 10 µm; with q/m value of $-3 \cdot 10^{-2}$ C/kg; in (a, b) no contamination on grounded pixels occurs in contrast to (c) (Löffler et al., 2011) (Reprinted with permission)

Intuitively, one would expect that particles with a higher q/m value are easier to manipulate by electrical fields and therefore should yield a better deposition quality. This, however, is not the case: A higher q/m value combined with a larger inert mass will cause particles to divert from their appointed path, determined by the electrical field configuration. Therefore, the impact of the selective force of the chip declines and the deposition quality decreases.

Concluding from the results, we reason that highly charged particles are an intrinsic characteristic of the aerosol created in our experiments. In fact, the critical surface charge density (i.e. electrical breakdown occurs) between two parallel metal plates, is invalid for dielectric particles. Due to the curvature of the particle surface and the dielectric character, higher electrical surface fields are possible without electrical breakdown.

Summarizing this section, a greater particle diameter together with higher triboelectric charge will cause contaminations in this present case of spatial defined particle deposition by means of an aerosol.

4.3.4 Stopping distance

Using a different approach, the impact of the particle diameter on the deposition process can be also demonstrated qualitatively. The stopping distance S of a particle, which is defined as the product of initial particle velocity v_0 and the relaxation time τ of a particle, which in turn is the time needed, until a particle with no initial velocity, released into a moving fluid, reaches $(1 - 1/e) \approx 63.2$ % of its final velocity v_f. Thus, the relaxation time is defined as (Hinds, 1999):

$$\tau = \rho_{part} \times d^2 \times C_c / (18 \times \eta_{air}), \tag{3}$$

where ρ_{part} is the density of the particle matrix and d is the particle diameter, η_{air} is the dynamic viscosity of the air. C_c is the phenomenological Cunningham correction factor, which can be approximated as $C_c = 1 + 1.14 \cdot K_n$ for particle diameters greater or equal than 1 µm. The Knudsen number is defined as $K_n = \lambda / (d/2)$, it is the quotient of the mean free path λ of the fluid and the particle radius d/2. As shown in Table 3, the stopping distance decreases rapidly with the particle diameter, resulting in a lower overall number of deposition events on the chip surface with decreasing diameter.

d [µm]	Kn	Cc	τ [s]	S(v= 1 m/s) [µm]
3	0.04	1.05	28.10-06	28
5	0.03	1.03	77.10-06	77
10	0.01	1.01	305.10-06	30

Table 3. The stopping distance S for particles with the diameters d and corresponding Knudsen number K_n with the Cunningham correction factor C_c; initial particle velocity is v = 1m/s

Resulting from the short stopping distance of smaller particles, these particles are easier to manipulate by electrical fields, resulting in highly precise particle deposition as shown in the simulations (Figure 16a, b and 17a, b).

4.3.5 Restriction of deposition layer thickness

An important restrictive effect in the selective particle deposition is illustrated in Figure 18: A simulation of particles with a diameter of 5 µm is shown. In Figure 18a and b, a 10 µm thick pre-deposited particle layer is shown, represented by a black rectangle with a surface charge of $2.7 \cdot 10^{-5}$ C/m² (a) and $5.4 \cdot 10^{-5}$ C/m² (b), which represents the possible surface charge range of a deposited particle layer. Fewer particles are deposited on the 100 V pixel in the bottom left picture, because of the increased repulsive force of the particle layer. In Figure 18 c and d, a 20 µm thick pre-deposited particle layer is shown, again represented by a black rectangle with a surface charge of $2.7 \cdot 10^{-5}$ C/m² (c) and $5.4 \cdot 10^{-5}$ C/m² (d). Here, the effect of the particle layer becomes more dominant (c) and eventually prevents any further particle deposition on the 100 V pixel. Moreover, in (d), one particle trajectory ends on an adjacent 0 V pixel, causing contamination.

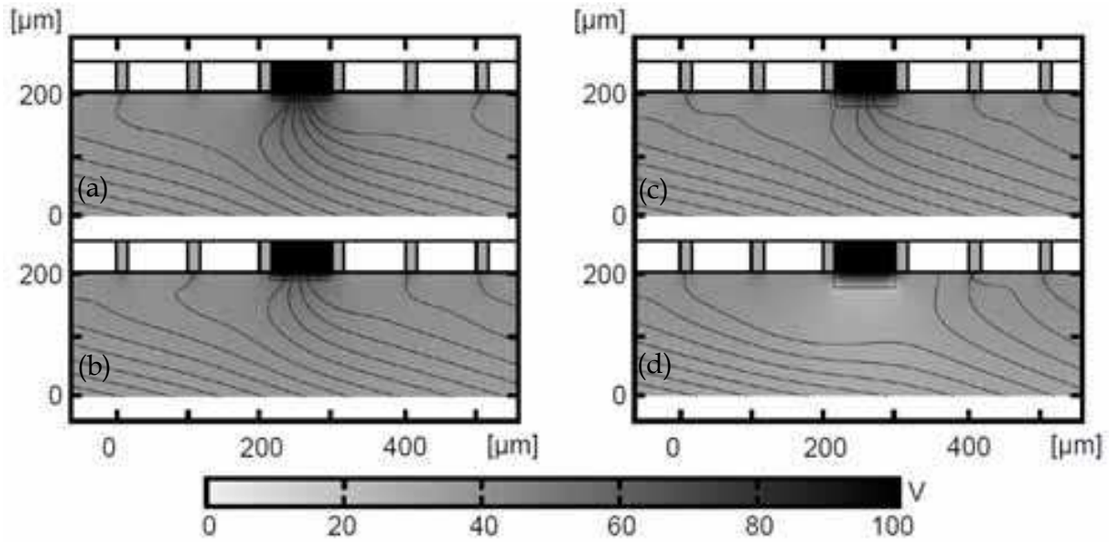

Fig. 18. Simulation of particles with a diameter of 5 µm, deposited onto a chip; (a, b) show a 10 µm particle layer (black rectangle), surface charge is $2.7 \cdot 10^{-5}$ C/m² (a) and $5.4 \cdot 10^{-5}$ C/m² (b); (c, d) show a 20 µm particle layer, surface charge is $2.7 \cdot 10^{-5}$ C/m² (c) and $5.4 \cdot 10^{-5}$ C/m² (d).

These simulations imply that it is not only important to study the selective effect on single particles: Especially the effect of already deposited particles on afterwards following particles is not yet fully investigated. Experiments suggest that the selectivity of the CMOS chip slowly declines with increasing particle load on the chip surface. Thus, each pattern has a critical limit of maximum particle load, where further particle deposition will lead to contaminations on the chip surface. Hence, it will be a topic of future research.

4.3.6 Improvements and consistency of experiments with simulations

Concluding from the preceding simulations, this section shows the improvements achieved by applying the theoretical results in practical particle deposition.

In Figure 19 left, a deposition pattern of four different deposition patterns (chess board, 1 of 16, 1 of 36, 1 of 64) of particles with a mean diameter of 15.6 µm is shown. A lot of contaminating particles are visible. In comparison, Figure 19 right shows the same deposition pattern, but with a mean particle diameter of only 2.3 µm, it is almost free of contaminations.

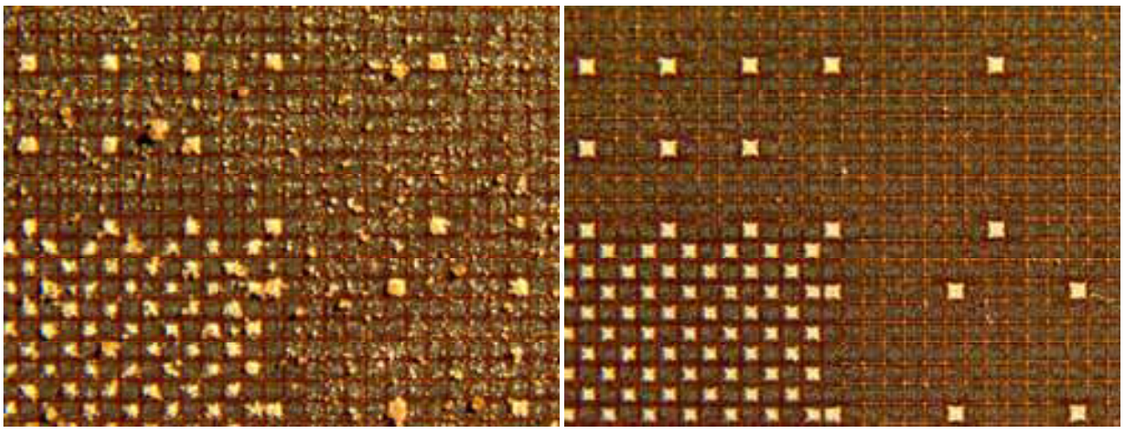

Fig. 19. Four different deposition patterns of micro particles on each chip surface: (left) high degree of contamination wide particle size distribution, mean diameter 15.6 µm; (right) almost free of contamination; mean particle diameter 2.3 µm

To illustrate the consistency of simulations and experiments, we simulated the electric potential of a detail of the chip surface. In Figure 20 left, a simulation of a 5 x 5 pixel checkerboard pattern on the CMOS chip surface is shown. Only the highest electric potential (between 99.8 V and 100 V) is shown in yellow, pixels are colored in grey, the grid electrode is shown in brown. In Figure 20 right, the experimental result of particle deposition with a diameter of 2.3 µm on the CMOS chip is shown. The particle deposition clearly resembles the simulation of the highest electric potential, small particles tend to be deposited in good agreement with the selective electrical field. Even the pincushion shape (effect described in Löffler et al., 2011) of the on the pixels deposited particles can be found in both cases.

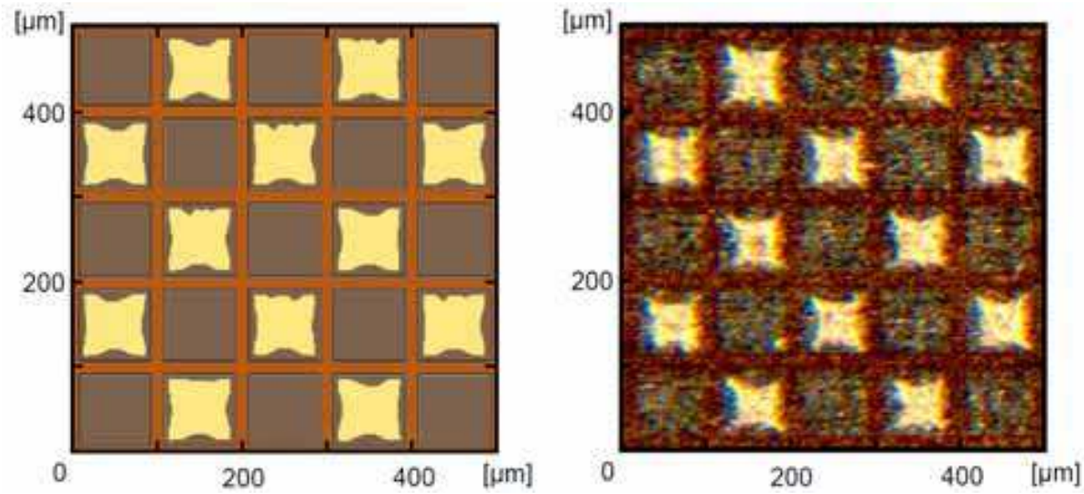

Fig. 20. (left) Simulation of a checkerboard pattern on the CMOS chip surface, only the highest electric potential (99.8 - 100 V) is shown in yellow, pixels are grey, the grid electrode is shown in brown; (right) experimental result of particle deposition (mean diameter of 2.3 µm)

4.4 Particle-based synthesis on microelectronic chips

The first successful proof-of-principle peptide synthesis (Nesterov-Müller, 2008) with amino acid particles was conducted on passive chips (see section 4.2). Two kinds of peptides NH_2-DYKDDDDK-substrate and NH_2-YPYDVPDYA-substrate were synthesized in a chess-board like pattern. Here, the letters are the standard notation for the amino acids: D is aspartic acid, Y tyrosine, K lysine, P proline, V valine, and A alanine. The first peptide can be recognized by the monoclonal mouse antibody called anti-FLAG. The second peptide epitope is an amino acid sequence characteristic for the hemagglutinin (HA) – a protein found on the surface of the influenza virus. Six different aerosol chambers were used according to the number of different amino acids. Two kinds of particles were deposited per layer. After the peptide synthesis as described in section 3, the chip was exposed to the antibodies to anti-FLAG and anti-HA antibodies which were stained with fluorescent labeled secondary antibodies. Alexa Fluor 488 and Alexa Fluor 546 (fluorescein derivates) were used as tag molecules for detection of the binding events. Finally, the chip was processed by the standard microarray scanner (Axon scanner GenePix 4000A) usually applied for the fluorescence measurement of the DNA microarrays. The results of immunostaining confirmed the principle possibility of fabrication of the peptide epitopes on the microelectronic chips. Lately, the same experiment has been repeated on the CMOS chip (Figure 21)[3]. Prior to the synthesis, the chips have been coated with a ca. 100-nm thick copolymer layer of 80% MMA (methylmethacrylate) and 20% PEG (poly(ethyleneglycol)methylmethacrylate). This layer has two functions: it protects the surface of the microelectronic chips – silicon nitride and aluminum electrodes against the chemicals used by peptide synthesis and serves at the same time as covalent binding partner for the initial amino acid groups.

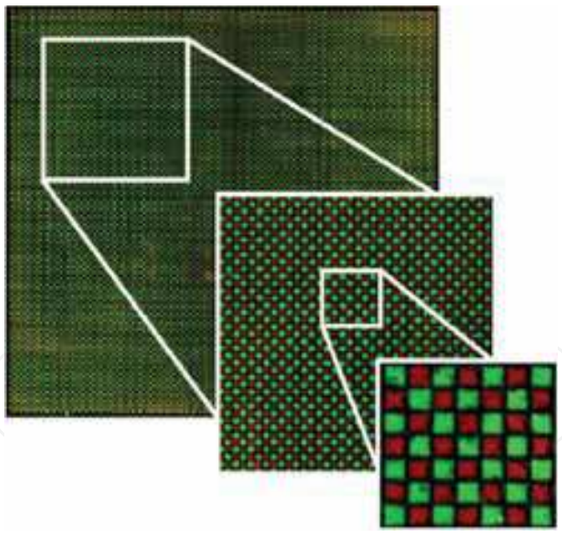

Fig. 21. Fluorescence scan of CMOS chip with Flag (green) and HA (red) epitopes synthesized and fluorescence-labelled by appropriate antibody combinations. The image was merged from two fluorescence scans at different wavelengths, contrast and brightness were adjusted. Pixel pitch is 100 μm. This demonstrates the high uniformity of signals and signal intensities over the whole chip and the compact coverage of all pixels (König et al., 2010).

[3]Reprinted from Sens. Act. B: V. 147, K König et al. Programmable high voltage CMOS chips for particle-based high-density combinatorial peptide synthesis, 418-427 (2010) with permission from Elsevier.

Specially designed Teflon chambers were used to protect the bonding wires of the chip and the PCB support during the peptide synthesis.

4.5 Chip printer

The peptide synthesis on the chip has several disadvantages. After 10-15 synthesis cycles and the removal of the protective groups with trifluoroacetic acid in the last step, the chip cannot be recycled for the synthesis of new arrays. This obstacle is not practical at today's manufacturing cost of high voltage microelectronic chips (up to 500 Euro/mm² manufacturing cost in the many project wafers run[4]). The chip cannot be separated from its PCB support and thus requires a relatively complicated Teflon protection during the peptide synthesis. The other drawback is that the size of the surface of the chip is limited by the technical process. Thus, a considerable part of this expensive surface should be reserved for mechanical Teflon protection contact (see black margins on the chip surface in Figure 11).

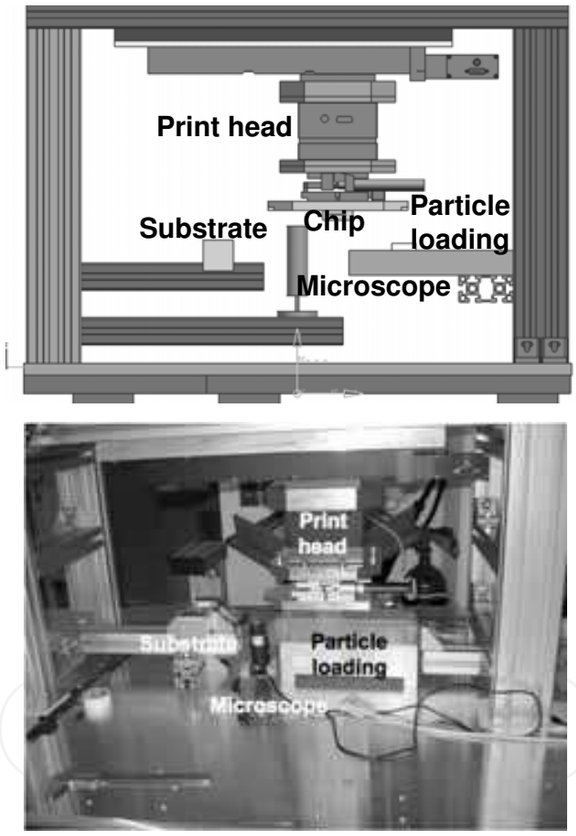

Fig. 22. Chip printer, (top) schematic drawing and (bottom) photo

Hence, a CMOS-chip-based xerographic printing machine (Cheng et al., 2010) has been developed to allow for the combinatorial particle deposition on dielectric surfaces (Figure 22). The CMOS chip is used as a printing head in this machine. The chip is mounted onto a tilt stage, which can be moved in the x, y, and z direction. The combinatorial deposition of particles consists of three steps: First, the electrical field pattern is generated on the surface

[4] http://www.europractice-ic.com/docs/MPW2011-general-v2.pdf

of the chip. Afterwards, the latent image is developed by contacting the chip with the bioparticle aerosol. These two steps can be repeated until the complete chip surface is covered with the desired particle pattern consisting of all 20 different amino acid particles. Finally, the particle pattern is transferred to a dielectric surface, e.g. a glass slide, by applying a homogenous electric field between the chip and an electrode on the backside of the dielectric support. Figure 23 shows an example of a bioparticle pattern transfer from the chip surface to a glass slide.

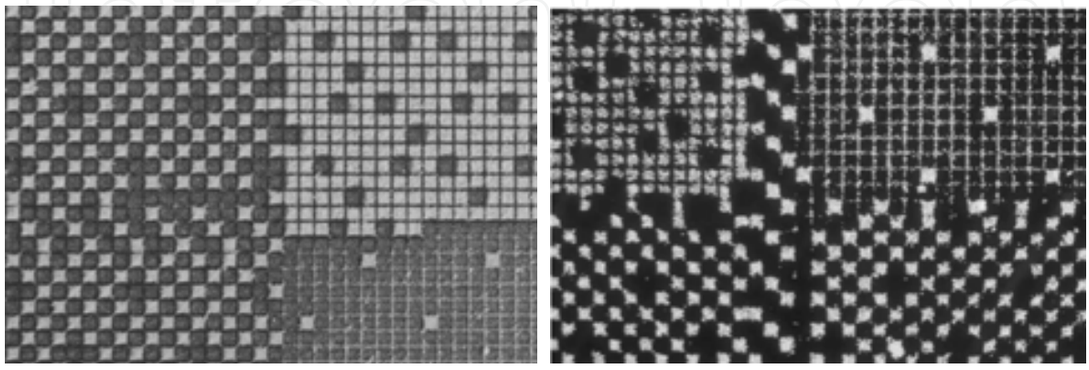

Fig. 23. (left) Amino acid particles selectively deposited on a chip; (right) amino acid particles printed onto a glass slide

5. Outlook

In this chapter, we have considered the three characteristics of biofunctional xerography: bioparticles, combinatorial particle deposition and solid phase peptide chemistry. While the solid phase peptide chemistry is a well established research field in biochemistry, biofunctional xerography remains an ambitious field with many possibilities for further development. Due to the rapid development in particle technology, particle parameters as shape, size distribution and electricity can nowadays be widely varied and adjusted to the specific application. Novel gentle particle production methods as a spray drying can be used to fabricate composite particles with activated monomers or even biopolymers inside. The use of particles with artificial monomers can stimulate the development of novel reaction schemes in the solid chemistry.

As already mentioned, the complexity of molecular arrays produced with biofunctional xerography is determined by the complexity of deposited particle patterns. Hence, there is still a large need for the development of methods for combinatorial particle deposition. The aim of this study should be, in the ideal case, a method of free combinatorial patterning of submicrometer particles with high spot densities up to a million spots per cm^2. The reported chip-based methods and the nanoxerography are very promising approaches. Also, we should not forget that xerography is still not exhausted by the electrophotographical principle used in modern laser printers. Less known are magnetography, photoconductography, photoactive pigment electrography et cetera, which proved to be non-competitive in imaging systems, but could be an interesting option for functional printing.

Driven by the idea to obtain more and cheaper peptides for antibody profiling and peptide diagnostics, biofunctional xerography emerged as a method for a large-scale synthesis of

peptide arrays. We suppose that biofunctional xerography will become an efficient method for the construction of molecular machines in a trial-and-error process and for the search of artificial molecules with properties of broad interest. Obviously, biofunctional xerography can be applied to fabricate high density arrays of artificial molecules such as PNA, peptoides, oligoureas or metallopeptides. All these molecules possess a modular structure with well defined distances between atoms and chemical groups. Thus, varying the residues of synthesized polymers, one can systematically study in high density array format the dependence of electrical, chemical, and optical properties of materials. Measuring the response to variations and improving it with an evolutionary method by combinatorially mutating the found molecules, one can create an unforeseen diversity in biofunctional polymers.

6. Acknowledgment

We thank K. König (currently at ABB Ladenburg) and H. Richter (Institute for Microelectronics Stuttgart) for the design of the chips used in the experiments. Furthermore, we thank our colleagues M. Beyer, I. Block, T. Felgenhauer, S. Fernandez, K. Leibe, G. Torralba, M. Hausmann, U. Trunk, V. Lindenstruth and V. Stadler whose contributions are cited in this chapter. Also we thank D. Rambow, J. Kretschmer, and S. Heß for technical assistance. We gratefully acknowledge the funding of the Baden-Württemberg Stiftung.

7. References

Adler, M. (1999). *Sprüheinbettung von Proteinen in Gerüstbildner: Stabilität und Oberflächenanalyse*. Dissertation Pharmazeutische Technologie. Nürnberg, Universität Erlangen.

Beyer, M.,* Nesterov, A.,* Block, I., König, K., Felgenhauer, T., Fernandez, S., Leibe, K., Torralba, G., Hausmann, M., Trunk, U., Lindenstruth, V., Bischoff, F.R., Stadler, V. & Breitling, F. (2007). Combinatorial synthesis of peptide arrays onto a computer chip's surface. *Science* 318, 1888; *shared 1st author.

Borsenberger, P. M. & Weiss, D. S. (1993). Organic photoreceptors for imaging systems. Marcel Dekker, New York.

Cezari, M. H. S. & Juliano, L. (1996). Studies on lactam formation during coupling procedures of N alpha-N omega-protected arginine derivatives. *Peptide research* 9(2), 88-91.

Cheng, Y.C., Löffler, F., König, K., Nesterov, A., Dörsam, E. & Breitling, F. (2010). Chip printer. *Proceedings of the 2nd WSEAS International Conference on Nanotechnology*. ISSN: 1790-5117, 19-22.

Coulson, J. M. & Richardson, J. F. (1999). Motion of Particles in a Fluid, In: *Particle Technology and Separation Processes*, Ch. 3. Chemical Engineering vol. 2, Oxford: Butterworth-Heinemann.

Desai, A., Lee, S.-W. & Tai, Y.-C. (1999). A MEMS electrostatic particles transportation system. *Sensors and Actuators* 73, 37-44.

Fodor, S.P., Read, J.L., Pirrung, M.C., Stryer, L., Lu, A.T., & Solas, D. (1991). Light-directed, spatially addressable parallel chemical synthesis. *Science* 251, 767–773.

Frank, R. (1992) Spot synthesis: An easy technique for the positionally addressable, parallel chemical synthesis on a membrane support. *Tetrahedron* 48, 9217–9232.

Fudouzi, H., Kobayashi, M. & Shinya, N. (2002). Site-Controlled Deposition of Microsized Particles Using an Electrostatic Assembly. *Adv. Mater.* 14, 1649-1652.

Hinds, W.C. (1999). *Aerosol Technology*. New York: Wiley Interscience.

Hughes J.F. (1984). *Electrostatic Powder Coatings*. Research Studies Press.

Jacobs, H.O., Campball, S.A. & Steward, M.G. (2002). Approaching nanoxerography: The use of electrostatic forces to position nanoparticles with 100 nm scale resolution *Adv. Mater.* 12, 1553-1557.

Jacobs, H.O. & Whitesides, G.M. (2001). Submicrometer pattering of charge in thin-film electrets. *Science* 291, 1763-1766.

Jakubke, H.D. & Jeschkeit, H. (1973). *Aminosäuren-Peptide-Proteine*. Berlin: Akademie-Verlag.

Jones, J. (2002). *Oxford Chemistry Primers*. Oxford University Press, Oxford, pp. 1-92.

König, K., Block, I., Nesterov, A., Torralba, G., Fernandez, S., Felgenhauer, T., Leibe, K., Schirwitz, C., Löffler, F., Painke, F., Wagner, J., Trunk, U., Bischoff, F.R., Breitling, F., Stadler, V., Hausmann, M. & Lindenstruth, V. (2010). Programmable high voltage CMOS chips for particle-based high-density combinatorial peptide synthesis. *Sens. Act. B*, 147, 418-427.

Löffler, F., Wagner, J., König, K., Märkle, F., Fernandez, S., Schirwitz, C., Torralba, G., Hausmann, M., Lindenstruth, V., Bischoff, F.R., Breitling, F. & Nesterov, A. (2011). High-precision combinatorial deposition of micro particle patterns on a microelectronic chip. *Aerosol Science and Technology*, 45, 65–74.

Merrifield, R.B. (1963). Solid Phase Peptide Synthesis. I. The Synthesis of a Tetrapeptide. *Journal of the American Chemical Society*, 85, 2149.

Nesterov, A., Löffler, F., König, K., Trunk, U., Leibe, K., Felgenhauer, T., Bischoff, F.R., Breitling, F., Lindenstruth, V., Stadler, V. & Hausmann, M. (2007). Measurement of triboelectric charging of moving micro particles by means of an inductive cylindrical probe. *Journal of Physics D Appl. Phys.* 40, 6115-6120.

Nesterov, A., Löffler, F., König, K., Trunk, U., Leibe, K., Felgenhauer, T., Stadler, V., Bischoff, F.R., Breitling, F., Lindenstruth, V. & Hausmann, M. (2007). Non - contact charge measurement of moving microparticles contacting dielectric surfaces. *Review of Scientific Instruments*, 78, 075111.

Nesterov-Müller, A. (2008). *Physical Aspects of Combinatorial Fabrication and Processing of Microchip Based Peptide Libraries*, Habilitation, Universität Heidelberg.

Nesterov, A., Löffler, F., Hausmann, M., Stadler, V., Bischoff, F.R. & Breitling, F. (2010). Manipulation of solid particle aerosols for combinatorial fabrication of molecular libraries. *SPIE Proc. ILLA'09*, ISSN: 1314-068X, Smolyan, October 18-22, 2009, 332-341.

Novick, V.J., Hummer, C.R., Dunn, P.F. (1989). Minimum electric field requirements for removing powder layers from a conductive surface. *J of Appl. Phys.* 65, 3242-3247.

Koch, J. & Mahler, M. (2002). *Peptide Arrays on Membrane Support*. Springer.

Stadler, V., Felgenhauer, T., Beyer, M., Fernandez, S., Leibe, K., Güttler, S., Gröning, M., König, K., Torralba, G., Hausmann, M., Lindenstruth, V., Nesterov, A., Block, I., Pipkorn, R., Poustka, A., Bischoff, F.R. & Breitling, F. (2008). Combinatorial synthesis of peptide arrays with a laser printer, *Angew. Chem. Inter. Ed.* 47, 7132.

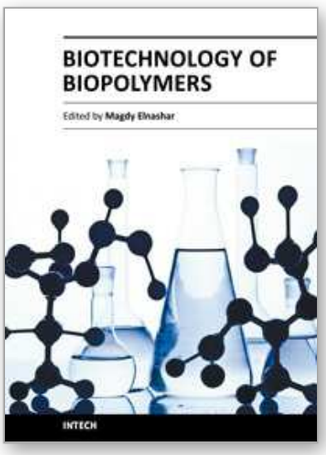

Biotechnology of Biopolymers

Edited by Prof. Magdy Elnashar

ISBN 978-953-307-179-4
Hard cover, 364 pages
Publisher InTech
Published online 24, June, 2011
Published in print edition June, 2011

The book "Biotechnology of Biopolymers" comprises 17 chapters covering occurrence, synthesis, isolation and production, properties and applications, biodegradation and modification, the relevant analysis methods to reveal the structures and properties of biopolymers and a special section on the theoretical, experimental and mathematical models of biopolymers. This book will hopefully be supportive to many scientists, physicians, pharmaceutics, engineers and other experts in a wide variety of different disciplines, in academia and in industry. It may not only support research and development but may be also suitable for teaching. Publishing of this book was achieved by choosing authors of the individual chapters for their recognized expertise and for their excellent contributions to the various fields of research.

INTECH
open science | open minds

InTech Europe
University Campus STeP Ri
Slavka Krautzeka 83/A
51000 Rijeka, Croatia
Phone: +385 (51) 770 447
Fax: +385 (51) 686 166
www.intechopen.com

InTech China
Unit 405, Office Block, Hotel Equatorial Shanghai
No.65, Yan An Road (West), Shanghai, 200040, China
中国上海市延安西路65号上海国际贵都大饭店办公楼405单元
Phone: +86-21-62489820
Fax: +86-21-62489821

IntechOpen